Mobile impurity in a Fermi sea from the functional renormalization group analytically continued to real time

Kazuhiko Kamikado,[1] Takuya Kanazawa,[2] and Shun Uchino[3,*]
[1]*Department of Physics, Tokyo Institute of Technology, Meguro, Tokyo 152-8551, Japan*
[2]*iTHES Research Group and Quantum Hadron Physics Laboratory, RIKEN, Wako, Saitama 351-0198, Japan*
[3]*RIKEN Center for Emergent Matter Science, Wako, Saitama 351-0198, Japan*
(Received 20 June 2016; published 17 January 2017)

Motivated by experiments with cold atoms, we investigate a mobile impurity immersed in a Fermi sea in three dimensions at zero temperature by means of the functional renormalization group. We first perform the derivative expansion of the effective action to calculate the ground-state energy and Tan's contact across the polaron-molecule transition for several mass imbalances. Next we study quasiparticle properties of the impurity by using a real-time method recently developed in nuclear physics, which allows one to go beyond the derivative expansion. We obtain the spectral function of the polaron and the effective mass and quasiparticle weight of attractive and repulsive polarons, and clarify how they are affected by mass imbalances.

DOI: 10.1103/PhysRevA.95.013612

I. INTRODUCTION

The concept of quasiparticles has become a cornerstone of quantum many-body physics. One of the fundamental problems is understanding the properties of a *polaron*, a single mobile impurity in a bath of majority particles [1–4]. While such an impurity effectively behaves as a free particle, renormalization effects due to interactions between the impurity and the bath are known to be significant.

The polaron problem had been discussed originally in the context of solid-state physics, where an electron interacts with a bath of phonons, that is, bosons [5]. Recently, experiments with ultracold atoms have allowed us to consider a similar problem with fermions: an impurity immersed in a bath of fermions [6,7]. Experiments using a mixture of two different hyperfine states as well as a heteronuclear mixture have been performed in two and three dimensions [8–11]. The s-wave scattering length characterizing the interaction between impurities and fermions in the bath can be tuned via the Feshbach resonance (FR) technique. This opens up a way to realize a novel strongly coupled impurity system, whose understanding requires a nonperturbative analysis.

A number of techniques in quantum many-body physics have been applied to the analysis of the polaron problem. A recently developed powerful numerical scheme, called the diagrammatic Monte Carlo (diagMC) method, was successfully applied to the broad-FR case [12–15]. Analytical methods including a variational calculation and a many-body T-matrix approach were also employed [16–26].

The functional renormalization group (FRG) based on an exact flow equation [27–31] offers an alternative route to tackling quantum many-body problems. Since the FRG is built on a philosophy different from that of the conventional methods above, approximations in the FRG may provide new insights into the mobile impurity problem. In [32], Schmidt and Enss examined this problem in the broad-FR limit using a Blaizot–Méndez-Galain–Wschebor (BMW)-type FRG [33] combined with the Padé approximation for analytic continuation to real time [34]. Their approach yields accurate results at imaginary time, but it comes at a high computational cost.

In this paper, we study the Fermi polaron problem using the FRG based on the derivative expansion, which is numerically much less expensive than the BMW approach. While the derivative expansion of the scale-dependent effective action is able to capture critical phenomena accurately [29,30], it is inadequate to describe the spectral properties of quasiparticles because it fails to capture higher excited states and a continuum incoherent background. Recently, however, a scheme to circumvent such difficulties of the derivative expansion on the basis of analytic continuation of flow equations to real time has been developed and tested in nuclear physics [35–38]. In this work, we apply this scheme to the polaron problem at zero temperature and reveal not only the thermodynamic properties of the system but also the spectral properties of quasiparticles including highly excited states, thus going far beyond the conventional realm of a derivative expansion. We remark that this is the first application of this scheme to a nonrelativistic, experimentally accessible system. This provides a viable alternative to other renormalization-group-based approaches to nonequilibrium physics [39,40].

This paper is organized as follows. In Sec. II we present our model Hamiltonian. In Sec. III we explain the elements of the FRG and describe flow equations in our formulation. Section IV reports our main results on thermodynamic and spectral properties of the Fermi polaron system. Section V is devoted to a summary. In the appendixes we discuss technical details of our formulation.

II. MODEL

We consider two-component fermions with an s-wave interaction. Since the s-wave scattering length is experimentally tuned via a molecule state in the closed channel, the natural model reflecting the microscopic dynamics of the FR is the

*shun.uchino@riken.jp

so-called two-channel model (with $\hbar = 1$),

$$S = \int_{\mathbf{x},\tau} \Bigg[\sum_{\sigma=\uparrow,\downarrow} \psi_\sigma^* \Big(\partial_\tau - \frac{\nabla^2}{2M_\sigma} - \mu_\sigma \Big) \psi_\sigma + \phi^* \Big(\partial_\tau - \frac{\nabla^2}{2M_\phi} - \mu_\phi \Big) \phi + h(\psi_\uparrow^* \psi_\downarrow^* \phi + \text{H.c.}) \Bigg], \quad (1)$$

where $\psi_\uparrow$ is the majority atom forming a noninteracting Fermi sea, $\psi_\downarrow$ is the impurity atom, ϕ is the molecule field made of $\uparrow$ and $\downarrow$ atoms, and $M_\phi = M_\uparrow + M_\downarrow$. The Yukawa (Feshbach) coupling h accounts for the formation and dissociation of molecules. Physically, h is related to the width of the FR. It is known [41,42] that the large-h limit corresponds to a broad FR where the scattering amplitude is described solely by the s-wave scattering length, while the small-h limit corresponds to a narrow FR where, in addition to the s-wave scattering length, the effective range is involved in the scattering amplitude. The chemical potential $\mu_\uparrow$ for the majority atoms is adjusted to the Fermi energy $E_F = k_F^2/(2M_\uparrow)$; the renormalization due to the impurity can be neglected in the thermodynamic limit. Determination of $\mu_\downarrow$ and μ_ϕ is discussed in subsequent sections.

In what follows, we use natural units $\hbar = 1$ and set

$$2M_\uparrow = 1, \quad 2M_\downarrow = \alpha, \quad \text{and} \quad 2M_\phi = 1 + \alpha. \quad (2)$$

III. FLOW EQUATIONS IN THE FUNCTIONAL RENORMALIZATION GROUP

The starting point of the FRG is the functional differential equation [27,28,43]

$$\partial_k \Gamma_k = \tfrac{1}{2} \text{STr} \big[\big(\Gamma_k^{(2)} + R_k \big)^{-1} \partial_k R_k \big], \quad (3)$$

where Γ_k and $\Gamma_k^{(2)}$ represent the average action at a scale k and an inverse of the two-point function, respectively. The symbol STr denotes the supertrace where the summation over momenta and frequencies, internal indices, and fields is taken. Note that in the supertrace, a minus sign for fermions is necessary. An important observation is that although the above flow equation has a one-loop structure, it contains the full field-dependent propagator and therefore allows one to incorporate nonperturbative effects.

The average action Γ_k includes all fluctuations with momenta $q \gtrsim k$. At the ultraviolet (UV) scale $k = \Lambda$, Γ_k reduces to the classical action, while at the infrared (IR) scale $k \to 0$, one obtains the full quantum effective action. These properties of the average action can be ensured through the use of a regulator function R_k, which possesses the following properties: $\lim_{k\to\infty} R_k(p) = \infty$, $\lim_{k\to 0} R_k(p) = 0$, and $\lim_{p\to 0} R_k(p) > 0$ [29]. While, in general, the flow equation itself depends on the choice of the regulator function,[1] the resultant physical properties in the IR limit are expected to be unaltered. In this paper, we choose the so-called three-dimensional sharp cutoff regulator: in the case of bosons, $R_k(p) = 0$ for $k \leqslant |\mathbf{p}|$ and $R_k(p) = \infty$ for $|\mathbf{p}| < k$. In the case of finite-density fermions, the cutoff should be imposed on momenta measured from the Fermi surface [45–47]. This sharp regulator is particularly useful in treating the flow equations analytically.

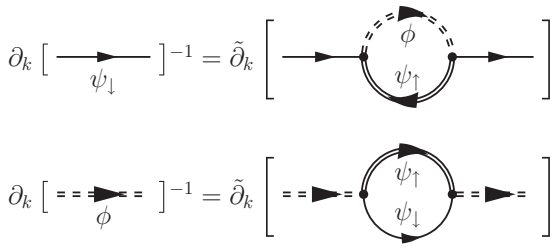

FIG. 1. Diagrams corresponding to the flow equations, (5), of the FRG. All the propagators in the loops are regularized with R_k.

As the exact flow equation, (3), is too complicated to solve exactly, some truncation procedure is practically required. We adopt the following truncation for the imaginary-time average effective action,

$$\Gamma_k = \int_P \big[\psi_\uparrow^* \big(-ip_0 + \mathbf{p}^2 - k_F^2 \big) \psi_\uparrow + \psi_\downarrow^* \mathscr{P}_{\downarrow,k}(P) \psi_\downarrow + \phi^* \mathscr{P}_{\phi,k}(P) \phi + h(\psi_\uparrow^* \psi_\downarrow^* \phi + \text{H.c.}) \big], \quad (4)$$

with $P = (p_0, \mathbf{p})$. Here, $\mathscr{P}_{\downarrow,k}$ and $\mathscr{P}_{\phi,k}$ are inverse propagators of the impurity and the molecule, respectively. For the sake of simplicity we omit the interactions $\psi_\uparrow^* \psi_\downarrow^* \psi_\downarrow \psi_\uparrow$ and $\psi_\uparrow^* \phi^* \psi_\uparrow \phi$ and neglect the renormalization of h.

By using the truncation, (4), we obtain the functional flow equations [32], depicted schematically in Fig. 1:

$$\partial_k \mathscr{P}_{\downarrow,k}(P) = h^2 \tilde{\partial}_k \int_Q G_{\phi,k}^c(Q) G_{\uparrow,k}^c(Q - P), \quad (5a)$$

$$\partial_k \mathscr{P}_{\phi,k}(P) = -h^2 \tilde{\partial}_k \int_Q G_{\downarrow,k}^c(Q) G_{\uparrow,k}^c(P - Q), \quad (5b)$$

where $\tilde{\partial}_k$ represents a derivative that acts only on the k dependence of the regulator R_k, and $G_k^c \equiv 1/(\mathscr{P}_k + R_k)$.

Solving (5) is a challenging numerical problem. Instead of solving these integrodifferential equations by brute force we proceed in two steps as follows [35–37]: in the first step, we solve (5) in the leading-order derivative expansion. In the second step, we substitute solutions obtained from the derivative expansion into the right-hand side of (5) and integrate both sides from $k = \Lambda$ to $k = 0$. In this way one can find $\mathscr{P}_k$ without assuming any specific ansatz for the form of $\mathscr{P}_k$. In principle, one may feed the obtained $\mathscr{P}_k$ into the right-hand side of (5) and integrate over k again. If this procedure is iteratively repeated sufficiently many times, one will gain exact solutions to (5). However, as previous analyses [35] indicate, the first iteration already yields reasonably accurate results and we explicitly demonstrate this in the following.

[1] For a detailed discussion of the use of four-dimensional regulators, see [44].

As the first step let us consider a truncation of $\mathscr{P}_k$ in the leading-order derivative expansion which respects the Galilean invariance of the theory,

$$\mathscr{P}_{\downarrow,k}(P) = A_{\downarrow,k}(-ip_0 + \mathbf{p}^2/\alpha) + m^2_{\downarrow,k}, \tag{6a}$$

$$\mathscr{P}_{\phi,k}(P) = A_{\phi,k}[-ip_0 + \mathbf{p}^2/(1+\alpha)] + m^2_{\phi,k}, \tag{6b}$$

where $A_{\downarrow,k}$ ($A_{\phi,k}$) and $m^2_{\downarrow,k}$ ($m^2_{\phi,k}$) represent the wave-function renormalization and gap for the impurity (the molecule), respectively. Then the regulated Green's functions read

$$G^c_{\uparrow,k}(P) = \frac{\theta\left(|\mathbf{p}^2 - k_F^2| - k^2\right)}{-ip_0 + \mathbf{p}^2 - k_F^2}, \tag{7a}$$

$$G^c_{\downarrow,k}(P) = \frac{\theta(|\mathbf{p}| - k)}{A_{\downarrow,k}(-ip_0 + \mathbf{p}^2/\alpha) + m^2_{\downarrow,k}}, \tag{7b}$$

$$G^c_{\phi,k}(P) = \frac{\theta(|\mathbf{p}| - k)}{A_{\phi,k}[-ip_0 + \mathbf{p}^2/(1+\alpha)] + m^2_{\phi,k}}, \tag{7c}$$

where $\theta(x)$ is the usual Heaviside step function.

Plugging (7) into (5) we straightforwardly obtain

$$\partial_k \mathscr{P}_{\downarrow,k}(P) = \frac{h^2 k}{4\pi^2 A_{\phi,k}}\left\{k\int_{-1}^{1} dx \frac{\theta\left(k_F^2 - 2k^2 - p^2 + 2pkx\right)}{-ip_0 + k_F^2 - p^2 + 2pkx - \frac{\alpha}{1+\alpha}k^2 + m^2_{\phi,k}/A_{\phi,k}}\right.$$
$$\left. + \sqrt{k_F^2 - k^2}\,\theta\left(k_F^2 - k^2\right)\int_{-1}^{1} dx \frac{\theta\left(k_F^2 - 2k^2 + p^2 + 2px\sqrt{k_F^2 - k^2}\right)}{-ip_0 + \frac{p^2 + \alpha k^2 + k_F^2 + 2px\sqrt{k_F^2 - k^2}}{1+\alpha} + m^2_{\phi,k}/A_{\phi,k}}\right\}, \tag{8a}$$

$$\partial_k \mathscr{P}_{\phi,k}(P) = \frac{h^2 k}{4\pi^2 A_{\downarrow,k}}\left\{k\int_{-1}^{1} dx \frac{\theta\left(p^2 - 2pkx - k_F^2\right)}{-ip_0 + p^2 - 2pkx - k_F^2 + \frac{1+\alpha}{\alpha}k^2 + m^2_{\downarrow,k}/A_{\downarrow,k}}\right.$$
$$\left. + \sqrt{k_F^2 + k^2}\int_{-1}^{1} dx \frac{\theta\left(k_F^2 + p^2 + 2px\sqrt{k_F^2 + k^2}\right)}{-ip_0 + \frac{k_F^2 + (1+\alpha)k^2 + p^2 + 2px\sqrt{k_F^2 + k^2}}{\alpha} + m^2_{\downarrow,k}/A_{\downarrow,k}}\right\}. \tag{8b}$$

To speed up numerical analysis we perform the remaining integral over x analytically with the formula

$$\int_{-1}^{1} dx \frac{\theta(a_1 + a_2 x)}{a_3 + a_2 x} = \Gamma(a_1, a_2, a_3), \tag{9}$$

where $a_1, a_2 \in \mathbb{R}$, $a_2 \neq 0$, $\mathrm{Im}\, a_3 \neq 0$, and

$$\Gamma(a_1,a_2,a_3) \equiv \frac{\theta(a_1 + |a_2|)}{|a_2|}\{\ln(|a_2| + a_3) - \ln[\max(0, a_1 - |a_2|) + a_3 - a_1]\}. \tag{10}$$

The resulting form of (8) is presented in Appendix A.

In units where $\hbar = 2M_\uparrow = 1$, all dimensionful quantities can be measured in units of the Fermi momentum k_F of the $\uparrow$ atoms. It is then useful to define

$$t \equiv \ln\frac{k}{k_F}, \quad \partial_t = k\frac{\partial}{\partial k}, \quad \hat{h} \equiv \frac{h}{\sqrt{k_F}},$$
$$\hat{m}_{\downarrow,k} \equiv \frac{m_{\downarrow,k}}{k_F}, \quad \hat{m}_{\phi,k} \equiv \frac{m_{\phi,k}}{k_F}. \tag{11}$$

The flow equations for $m_{\downarrow,k}$, $m_{\phi,k}$, $A_{\downarrow,k}$, and $A_{\phi,k}$ can be derived via expansion of (8) around the low-frequency and low-momentum limit. The results read

$$\partial_t A_\downarrow = -\theta(1 - 2e^{2t})\frac{\hat{h}^2 e^{2t}}{2\pi^2 A_\phi}\left[\frac{e^t}{\left(1 - \frac{\alpha}{1+\alpha}e^{2t} + \hat{m}^2_\phi/A_\phi\right)^2}\right.$$
$$\left. + \frac{\sqrt{1 - e^{2t}}}{\left(\frac{1+\alpha e^{2t}}{1+\alpha} + \hat{m}^2_\phi/A_\phi\right)^2}\right], \tag{12a}$$

$$\partial_t \hat{m}^2_\downarrow = \theta(1 - 2e^{2t})\frac{\hat{h}^2 e^{2t}}{2\pi^2 A_\phi}\left[\frac{e^t}{1 - \frac{\alpha}{1+\alpha}e^{2t} + \hat{m}^2_\phi/A_\phi}\right.$$
$$\left. + \frac{\sqrt{1 - e^{2t}}}{\frac{1+\alpha e^{2t}}{1+\alpha} + \hat{m}^2_\phi/A_\phi}\right], \tag{12b}$$

$$\partial_t A_\phi = -\frac{\hat{h}^2 e^{2t}}{2\pi^2 A_\downarrow}\frac{\sqrt{1 + e^{2t}}}{\left[\frac{1+(1+\alpha)e^{2t}}{\alpha} + \hat{m}^2_\downarrow/A_\downarrow\right]^2}, \tag{12c}$$

$$\partial_t \hat{m}^2_\phi = \frac{\hat{h}^2 e^{2t}}{2\pi^2 A_\downarrow}\frac{\sqrt{1 + e^{2t}}}{\frac{1+(1+\alpha)e^{2t}}{\alpha} + \hat{m}^2_\downarrow/A_\downarrow}. \tag{12d}$$

For $\alpha = 1$, Eqs. (12) reduce to Eq. (A2) in [32].

The initial conditions at the scale $k = \Lambda$ are given by

$$A_{\downarrow,\Lambda} = A_{\phi,\Lambda} = 1, \tag{13}$$

$$\hat{m}^2_{\downarrow,\Lambda} = -\hat{\mu}_\downarrow, \tag{14}$$

$$\hat{m}^2_{\phi,\Lambda} = \frac{\alpha}{4\pi(1+\alpha)}\hat{h}^2\left(\frac{2}{\pi}e^{t_0} - \frac{1}{k_F a}\right) - 1 - \hat{\mu}_\downarrow, \tag{15}$$

where $t_0 \equiv \ln(\Lambda/k_F)$. These initial conditions are derived in Appendix B for completeness. The value of $\hat{\mu}_\downarrow$ should be chosen so that $\mathrm{Min}(\hat{m}^2_{\downarrow,k=0}, \hat{m}^2_{\phi,k=0}) = 0$ [32]; see Sec. IV for a more precise explanation.

Once the solutions to (12) are obtained for all k, we substitute them into the right-hand side of (8) and then perform analytic continuation of (8) to real frequency ω via

$$p_0 = -i(\omega + i\varepsilon), \tag{16}$$

where $\varepsilon > 0$ is an infinitesimal constant (see Appendix A for flow equations at real frequency). Afterwards we integrate both sides of (8) from $k = \Lambda$ down to $k = 0$ and, finally, obtain the retarded two-point functions $\hat{\mathscr{P}}^{\mathrm{R}}_{\downarrow/\phi}(\hat{\omega}, \hat{p}) = \mathscr{P}^{\mathrm{R}}_{\downarrow/\phi}(\hat{\omega}, \hat{p})/k_F^2$ in Minkowski spacetime, with $\hat{\omega} \equiv \omega/k_F^2$ and $\hat{p} \equiv p/k_F$. The spectral functions are obtained as

$$\mathcal{A}_{\downarrow/\phi}(\hat{\omega}, \hat{p}) = \frac{1}{\pi}\mathrm{Im}\frac{1}{\hat{\mathscr{P}}^{\mathrm{R}}_{\downarrow/\phi}(\hat{\omega}, \hat{p})}. \tag{17}$$

They should not be confused with the wave-function renormalization $A_{\downarrow/\phi}$.

In this method, in which the analytic continuation is done directly at the level of the flow equation, one can entirely avoid a numerically expensive implementation of approximate analytic continuation of Euclidean correlators to real time, such as the Padé approximation [34] and the maximum entropy method [48]. In addition, we note that the computional time in this method is remarkably short. This is due to the fact that our flow equations consist only of $A_{\downarrow/\phi,k}$ and $m_{\downarrow/\phi,k}$, each of which can be determined with the derivative expansion, and we can analytically perform the integrals in momentum and frequency with Eq. (9). This is in contrast to the approach in Ref. [32], where one must take every point in the (ω, p) plane and perform the loop integral in flow equations numerically. These are the major advantages of the present scheme.

IV. RESULTS

In this section we proceed to numerical results. Parameters in the present model have been chosen as follows.

(i) The (normalized) inverse scattering length $(k_F a)^{-1}$ is varied from negative to positive values across the unitarity limit. This enables us to probe the polaron-molecule transition.

(ii) As for the mass ratio $\alpha = M_\downarrow/M_\uparrow$, we examine three cases, $\alpha = 6.6$, 1, and 0.5, covering both heavy and light impurities. In choosing $\alpha = 6.6 \simeq 40/6$ we have in mind ^{40}K atoms immersed in the Fermi sea of ^{6}Li atoms [10].[2]

(iii) In this work we limit ourselves to a broad-FR system, which corresponds to the large-h limit of (1) [41,42]. We have confirmed that the numerical results become insensitive to $\hat{h}$ provided $\hat{h} \gtrsim 150$. Throughout this section we choose $\hat{h} = 300$.

(iv) We set $\Lambda = 10^3 k_F$ as in [32], which implies

$$t_0 = \ln 10^3 \simeq 6.907. \tag{18}$$

The flows are solved for $t_{\mathrm{min}} \leqslant t \leqslant t_0$. The lower limit t_{min} should be chosen small enough to ensure convergence of the flow. In this work, we set $t_{\mathrm{min}} = -5.0$. We have confirmed that at t_{min}, all flowing parameters already reach asymptotic values; see Appendix C for an explicit check.

(v) We set $\hat{\varepsilon} \equiv \varepsilon/k_F^2 = 10^{-3}$ throughout this work. For completeness, the $\hat{\varepsilon}$ dependence of spectral functions is examined in Appendix D.

[2]We note that the experimental system of [10] corresponds to a narrow FR and, also, at nonzero temperature. Thus a direct comparison of [10] with our numerical results is not possible.

TABLE I. Polaron-molecule transition points for various mass imbalances.

α	Transition point
6.6	$(k_F a)^{-1} = 0.4006$
1.0	$(k_F a)^{-1} = 0.973$
0.5	$(k_F a)^{-1} = 1.390$

A. Thermodynamic properties

We first examine the thermodynamic properties of the impurity system. In order to realize a system with a single $\downarrow$ atom in the medium of $\uparrow$ atoms, we tune the chemical potential of the $\downarrow$ atom. The ground-state energy is determined as the *minimal* $\hat{\mu}^c_\downarrow$ that satisfies the following condition [32]:

$$\hat{m}^2_{\downarrow,k=0} \geqslant 0 \quad \text{and} \quad \hat{m}^2_{\phi,k=0} \geqslant 0 \quad \text{for} \quad \forall \hat{\mu}_\downarrow \geqslant \hat{\mu}^c_\downarrow. \tag{19}$$

If $\hat{m}^2_{\downarrow,k=0} = 0$ and $\hat{m}^2_{\phi,k=0} > 0$ at $\hat{\mu}_\downarrow = \hat{\mu}^c_\downarrow$, the system is on the polaronic side, i.e., forming a molecule is energetically more costly than forming a polaron. On the other hand, if $\hat{m}^2_{\downarrow,k=0} > 0$ and $\hat{m}^2_{\phi,k=0} = 0$ at $\hat{\mu}^c_\downarrow$, the system is on the molecule side and a molecule is formed in the ground state.

In Table. I, we summarize the resulting values of the polaron-molecule transition points where both the polaron and the molecule are gapless in the IR limit.

The tendency that the polaron-molecule transition moves to higher $1/(k_F a)$ for a lighter impurity is consistent with previous studies [19,26,49]. The polaron-molecule transition in our leading-order derivative expansion for $\alpha = 1$ occurs at $(k_F a)^{-1} = 0.973$, which compares well with the prediction of the diagMC, 0.90(2) [12,13], and that of the BMW-type FRG, 0.904(5) [32]. Close values are obtained in other approaches as well [14,19–21,24,26].

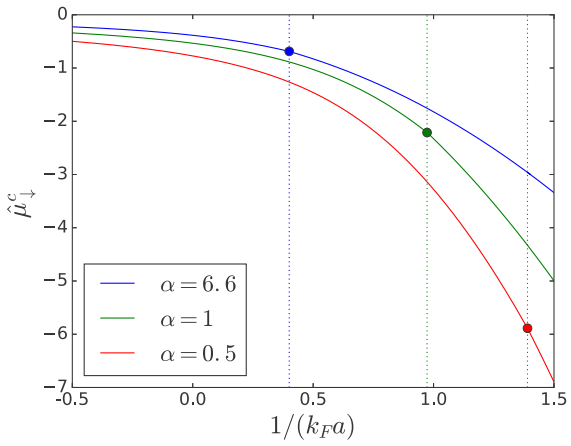

FIG. 2. Ground-state energy of the impurity system for $\alpha = 6.6$ (upper curve), $\alpha = 1$ (middle curve), and $\alpha = 0.5$ (lower curve). Dotted vertical lines represent the location of the polaron-molecule transition for each α.

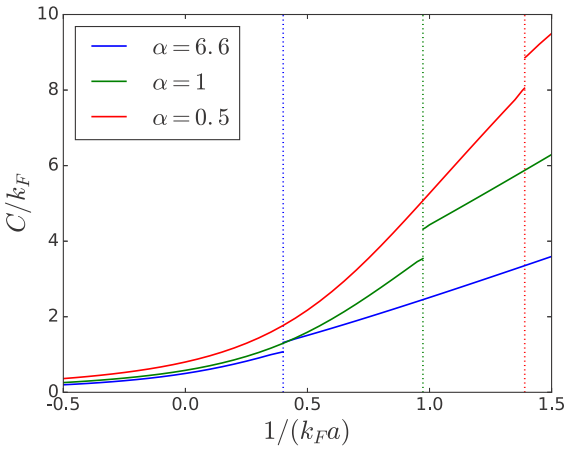

FIG. 3. Tan's contact for $\alpha = 0.5$ (upper curve), $\alpha = 1$ (middle curve), and $\alpha = 6.6$ (lower curve). Dotted vertical lines are the same as in Fig. 2.

Figure 2 displays the ground-state energy $\hat{\mu}_\downarrow^c$ of the impurity $\hat{\mu}_\downarrow^c$.[3] At the unitarity limit for $\alpha = 1$ we obtain $\hat{\mu}_\downarrow = -0.535$, which should be compared with $\hat{\mu}_\downarrow = -0.57$ [32] from the BMW-type FRG, $\hat{\mu}_\downarrow = -0.618$ [12] and -0.615 [13,14] from the diagMC, $\hat{\mu}_\downarrow = -0.6066$ from a variational method [16], and $\hat{\mu}_\downarrow = -0.6156$ from [17]. Furthermore, at $1/(k_F a) = 1.0$ with $\alpha = 1$, we obtain $\hat{\mu}_\downarrow = -2.33$, which lies slightly above the value -2.62 from [12–14]. In the case of a heavy impurity ($\alpha = 6.6$) at unitarity, we obtain $\hat{\mu}_\downarrow = -0.385$, not far away from the value -0.44 from the T-matrix approach [51]. In the case of a light impurity ($\alpha = 0.5$) at unitarity, we obtain $\hat{\mu}_\downarrow = -0.772$, to be compared with ~ -0.9 from the diagMC [15] and ~ -0.87 from a variational method [16].

Based on the above evaluation, we can determine the so-called Tan's contact, which is directly related to the slope of the ground-state energy:

$$C = 8\pi M_r a^2 \frac{dE}{da} = -8\pi M_r k_F \frac{d\hat{\mu}_\downarrow^c}{d[1/(k_F a)]}, \qquad (20)$$

where $M_r = (M_\uparrow^{-1} + M_\downarrow^{-1})^{-1}$ is the reduced mass. We refer to Appendix E for more details on (20). In Fig. 3, Tan's contact in a mobile impurity system is plotted. It clearly shows the first-order nature of the transition: since the slope of the ground-state energy is discontinuous at the polaron-molecule transition point, Tan's contact also shows a discontinuity [21]. A measurement of Tan's contact may be useful to determine the polaron-molecule transition experimentally.

B. Quasiparticle properties

Next we discuss the spectral properties of the impurity. In Fig. 4 we plot the spectral density of the polaron in an equal-mass system. There are two quasiparticle peaks [22]: the high-energy branch, called the *repulsive polaron*; and the lower-energy branch called the *attractive polaron*. Between these two peaks, there appears a molecule-hole continuum. These spectral features are consistent with previous studies [24,32,52]. We have also examined the spectral density in a mass-imbalanced system and found that it shares the same structure as in Fig. 4. In Fig. 5, we show the renormalization-group scale dependence of the spectral density of the polaron in an equal-mass system. For $t \geqslant -0.37$, the spectral density remains trivial or classical. At $t = -0.38$, the horizontal branch suddenly splits into two branches and a shallow continuum in between. After $t = -0.38$ the

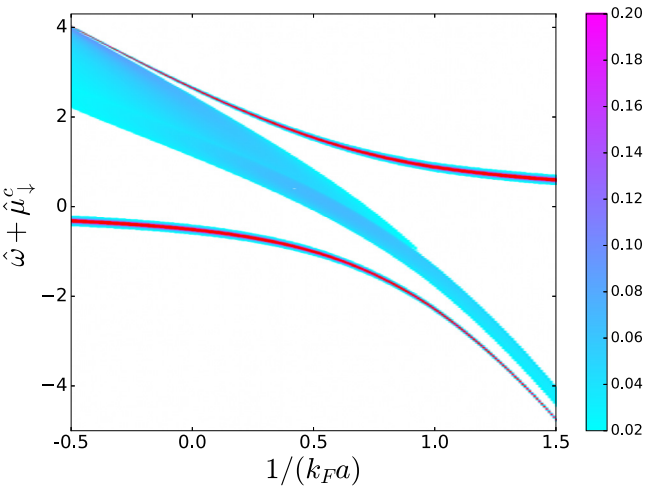

FIG. 4. Spectral density of the polaron at zero momentum $\mathcal{A}_\downarrow(\omega, \mathbf{p} = \mathbf{0})$ for $\alpha = 1$. $\mathcal{A}_\downarrow < 0.02$ ($\mathcal{A}_\downarrow > 0.2$) in the white (red) region.

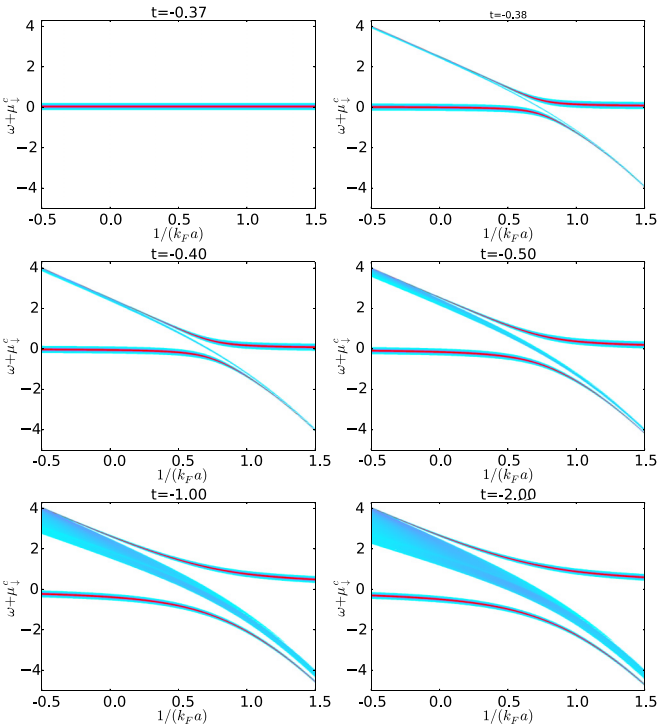

FIG. 5. Scale evolution of $\mathcal{A}_\downarrow(\omega, \mathbf{p} = \mathbf{0})$ for $\alpha = 1$. The color map is the same as in Fig. 4.

[3] We note that the ground-state energy in the FRG depends slightly on the choice of the regulator R_k [50].

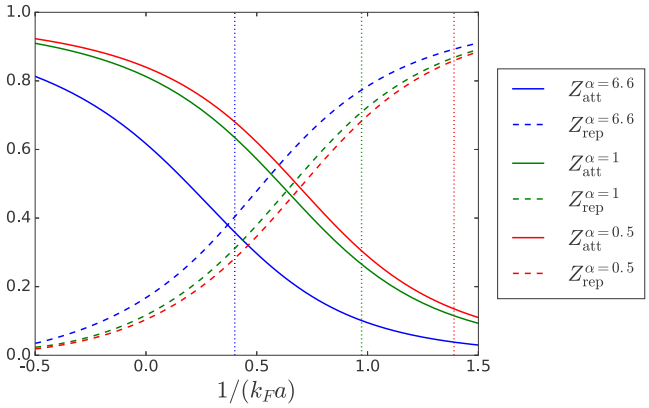

FIG. 6. Quasiparticle weight of the impurity for the attractive and repulsive branches. Upper (lower dotted), middle (dotted), and lower (upper dotted) curves represent, respectively, the results for $\alpha = 0.5$, $\alpha = 1$, and $\alpha = 6.6$. Dotted vertical lines represent the polaron-molecule transition for each α.

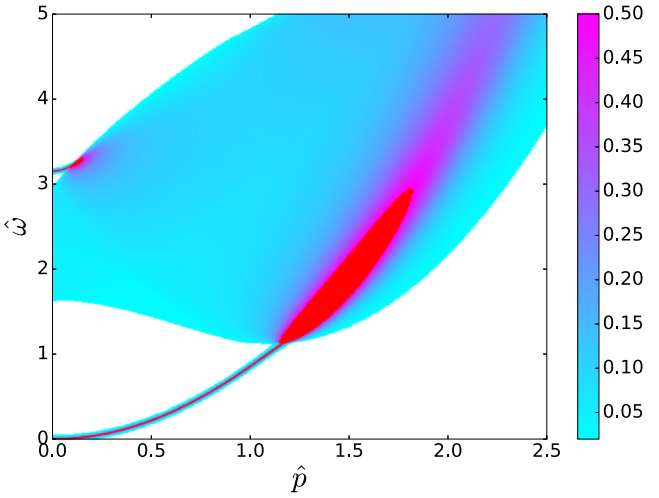

FIG. 7. $\mathcal{A}_\downarrow(\omega,\mathbf{p})$ for $\alpha = 1$ in the unitarity limit. $\mathcal{A}_\downarrow < 0.02$ ($\mathcal{A}_\downarrow > 0.5$) in the white (red) region.

two peaks are gradually deformed to the forms in the IR limit, while the molecule-hole continuum increases the width, especially on the polaron side, $1/(k_F a) \lesssim 1$. It is intriguing that both the repulsive polaron and the attractive polaron originate partly from the trivial unrenormalized spectrum in the UV.

The quasiparticle weights are calculated from the zeros of the real part of the two-point function in the IR limit. First, we numerically determine the peak positions of the attractive and repulsive polaron,

$$\mathrm{Re}\mathscr{P}_\downarrow^{\mathrm{R}}(\omega,\mathbf{p}=\mathbf{0})\big|_{\omega=\omega_{\mathrm{att/rep}}} = 0. \tag{21}$$

The energy of the repulsive polaron determined in this way was observed to converge to the asymptotic formula [53] for small positive $k_F a$. At the zeros, the quasiparticle weights are determined as

$$Z_{\mathrm{att/rep}} \equiv -[\partial_\omega \mathrm{Re}\mathscr{P}_\downarrow^{\mathrm{R}}(\omega,\mathbf{p}=\mathbf{0})]^{-1}\big|_{\omega=\omega_{\mathrm{att/rep}}}. \tag{22}$$

The above definition implicitly relies on the fact that the imaginary part of the $\mathbf{p} = \mathbf{0}$ two-point function at the zeros is vanishingly small in the present scheme at $\hat{\varepsilon} \ll 1$. (If the imaginary part is not small, the definition above is no longer valid and one needs to search for a quasiparticle pole on the complex ω plane.) Considering that the repulsive polaron is a high-energy metastable branch and naturally has a finite life time [22,24,32], the absence of the decay width may be an artifact of the present scheme.

In Fig. 6, we plot the quasiparticle weight of the attractive and repulsive polarons. On the molecule side, the repulsive polaron is dominant at every mass ratio. When the scattering length is shifted to the polaronic side, the weight of the repulsive polaron decreases and exchanges dominance with the attractive polaron. Note that the crossing of $Z_{\rm rep}$ and $Z_{\rm att}$ does not occur exactly at the polaron-molecule transition. These features of the weight Z are consistent with previous studies [14,21,24,32,49]. Quantitatively, for equal masses ($\alpha = 1$) at unitarity we obtain $Z_{\rm att} = 0.813$, which is close to the values of 0.78–0.80 from the variational method [21], the T-matrix method [49], and the BMW-type FRG [32], as well as the value of 0.7586(27) from the diagMC [14]. Note, however, that all of these results are well above the value 0.39(9) obtained in an experiment on ^{6}Li atoms [8]. In the case of a heavy impurity ($\alpha = 6.6$) at unitarity we obtain $Z_{\rm att} = 0.617$, which is close to the value of $\sim$0.64 from the T-matrix method [51] and the diagMC [15].

Next we discuss the nature of the quasiparticles at $\mathbf{p} \neq \mathbf{0}$. The polaron spectral density at finite momenta in the unitarity limit is shown in Fig. 7. At zero momentum, neither the attractive nor the repulsive polaron branch has a width. By contrast, at finite momentum, the peaks merge with the molecule-hole continuum and acquire a finite width. As the momentum increases, the branches lose sharp peaks and can no longer be clearly distinguished from the smooth continuum.

From the finite-momentum real-time correlation functions, we can extract the effective mass of the attractive and repulsive polarons: $m_{\downarrow\mathrm{att}}$ and $m_{\downarrow\mathrm{rep}}$. First, we determine the dispersion relation of the quasiparticles $E_{\mathrm{att/rep}}(\mathbf{p})$ by solving the equation

$$\mathrm{Re}\mathscr{P}_\downarrow^{\mathrm{R}}(\omega,\mathbf{p})\big|_{\omega=E_{\mathrm{att/rep}}(\mathbf{p})} = 0. \tag{23}$$

Then we fit the dispersion relation with the following fit function:

$$E_{\mathrm{att/rep}}(\mathbf{p}) - E_{\mathrm{att/rep}}(\mathbf{0}) = \frac{\mathbf{p}^2}{2m_{\downarrow\mathrm{att/rep}}} + O(p^4). \tag{24}$$

In Fig. 8, the effective mass of the attractive polaron is shown. At $(k_F a)^{-1} = -0.5$, the $m_{\downarrow\mathrm{att}}$ values for three α's are already close to the asymptotic value $M_\downarrow = \alpha/2$ in the free limit $k_F a \to 0^-$. For equal masses ($\alpha = 1$) at unitarity we find $m_{\downarrow\mathrm{att}}/M_\downarrow = 1.125$, which lies above the 1.04(3) [54] and 1.09(2) [55] from fixed-node diffusion Monte Carlo simulations but slightly below the 1.17 [16] and 1.197 [17] from variational methods and $\sim$1.18 from a T-matrix approach [49]. For equal masses at $1/(k_F a) = 1.0$, we find $m_{\downarrow\mathrm{att}}/M_\downarrow = 2.90$, which is between the value of $\sim$2.5

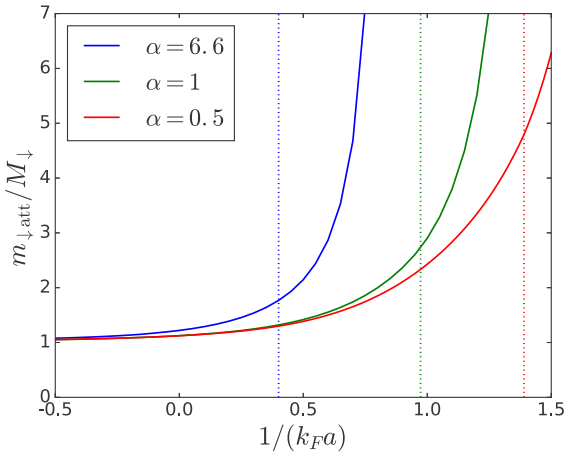

FIG. 8. Effective mass of the attractive polaron in units of the bare mass $M_{\downarrow} = \alpha/2$ for $\alpha = 6.6$ (upper curve), $\alpha = 1$ (middle curve), and $\alpha = 0.5$ (lower curve). The dotted vertical line represents the polaron-molecule transition for each α.

from a variational method [16] and the value of ∼3.5 from the diagMC [12,13]. In the case of a heavy impurity ($\alpha = 6.6$) at unitarity, we obtain $m_{\downarrow \mathrm{att}}/M_{\downarrow} = 1.22$, whereas the T-matrix approach yields 1.16 [51]. In the case of a light impurity at $1/(k_F a) = 1.0$, we find $m_{\downarrow \mathrm{att}}/M_{\downarrow} = 2.43$, while Ref. [19] reports ∼3.3.

At fixed $1/(k_F a)$, we found $m_{\downarrow \mathrm{att}}/M_{\downarrow}$ to be an increasing function of α, which agrees with [19] but disagrees with [16]. Overall, the effective mass monotonically increases across the polaron-molecule transition and eventually diverges at some point. Deep in the molecular region, we found $m_{\downarrow \mathrm{att}} < 0$ (not shown in Fig. 8), in agreement with [26]; this is consistent with the fact that the polaron is not a stable quasiparticle in this region.

We also calculated the effective mass of the repulsive polaron, finding that although $m_{\downarrow \mathrm{rep}}$ expectedly converges to the bare mass $\alpha/2$ at $1/(k_F a) \gg 1$, it *decreases* to 0 near the unitarity limit. The latter behavior contradicts other studies [24,49] showing an enhancement of $m_{\downarrow \mathrm{rep}}$ towards unitarity. This could indicate a shortcoming of the present scheme in a strongly interacting regime. For a small negative $1/(k_F a)$, we found that the repulsive polaron branch merges with the molecule-hole continuum even at small momenta, which makes $m_{\downarrow \mathrm{rep}}$ ill defined in this limit.

V. SUMMARY

We have examined a mobile impurity immersed in a Fermi sea realized in cold atoms. We have calculated thermodynamic quantities by means of the derivative expansion method in the FRG and obtained results that are in reasonable agreement with the diagMC simulations and other analytical methods.

The important aspect of the mobile impurity problem is that the spectral properties are rich since, in addition to the attractive polaron, the molecule-hole continuum and the repulsive polaron appear in higher frequency regimes. To extract spectral properties within the FRG, we have adopted a real-time method originally developed in nuclear physics and shown that it is successful in generating the spectral weights at high frequencies, which are difficult to obtain within the conventional derivative expansion method. The key point is solving the flow equations [Eq. (5)] in an iterative manner. Our analyses show that one iteration allows one to reproduce qualitative features in the Fermi polaron system. A quantitative agreement with the diagMC method may be obtained by additional iterations, whose implementation is an interesting future work. Applying our method to the other experimentally achievable systems such as the Bose polaron [56,57], the BCS-BEC crossover in two-component Fermi gases [58], and Bose-Fermi mixture systems [59,60] may also be interesting.

The polaron problem may be one of the best systems to analyze the accuracy and potential of a many-body technique, thanks to its experimental accessibility and the applicability of the diagMC method, in marked contrast to a number of models discussed in nuclear and particle physics. Our consideration may pave the way to an efficient algorithm in the real-time FRG.

ACKNOWLEDGMENTS

T.K. was supported by the RIKEN iTHES project. T.K. thanks P. Massignan for useful correspondence. S.U. thanks T. Enss for useful discussions. S.U. was supported by Grant for Basic Science Research Projects from The Sumitomo Foundation.

APPENDIX A: FLOW EQUATIONS FOR TWO-POINT FUNCTIONS

By means of the integration formula, (9), the flow equations, (8), are recast into the form

$$\partial_t \hat{\mathscr{P}}^{\mathrm{R}}_{\downarrow}(\hat{\omega},\hat{p}) = \frac{\hat{h}^2 e^{2t}}{4\pi^2 A_{\phi,k}} \left\{ e^t \Gamma\left(1 - 2e^{2t} - \hat{p}^2, 2\hat{p}e^t, 1 - \hat{p}^2 - \frac{\alpha}{1+\alpha} e^{2t} + \frac{\hat{m}^2_{\phi,k}}{A_{\phi,k}} - \hat{\omega} - i\hat{\varepsilon}\right) \right.$$
$$\left. + \theta(1 - e^{2t}) \sqrt{1 - e^{2t}}\, \Gamma\left(\frac{1 - 2e^{2t} + \hat{p}^2}{1+\alpha}, \frac{2\hat{p}\sqrt{1 - e^{2t}}}{1+\alpha}, \frac{1 + \hat{p}^2 + \alpha e^{2t}}{1+\alpha} + \frac{\hat{m}^2_{\phi,k}}{A_{\phi,k}} - \hat{\omega} - i\hat{\varepsilon}\right) \right\}, \tag{A1}$$

$$\partial_t \hat{\mathscr{P}}^{\mathrm{R}}_{\phi}(\hat{\omega},\hat{p}) = \frac{\hat{h}^2 e^{2t}}{4\pi^2 A_{\downarrow,k}} \left\{ e^t \Gamma\left(\hat{p}^2 - 1, -2\hat{p}e^t, \hat{p}^2 - 1 + \frac{1+\alpha}{\alpha} e^{2t} + \frac{\hat{m}^2_{\downarrow,k}}{A_{\downarrow,k}} - \hat{\omega} - i\hat{\varepsilon}\right) \right.$$
$$\left. + \sqrt{1 + e^{2t}}\, \Gamma\left(\frac{1 + \hat{p}^2}{\alpha}, \frac{2\hat{p}\sqrt{1 + e^{2t}}}{\alpha}, \frac{1 + \hat{p}^2 + (1+\alpha)e^{2t}}{\alpha} + \frac{\hat{m}^2_{\downarrow,k}}{A_{\downarrow,k}} - \hat{\omega} - i\hat{\varepsilon}\right) \right\}, \tag{A2}$$

where the analytic continuation, (16), has been performed. The above flow equations are solved under the initial conditions

$$\hat{\mathscr{P}}^{\mathrm{R}}_{\downarrow,\Lambda}(\hat{\omega},\hat{p}) = A_{\downarrow,\Lambda}(-\hat{\omega} - i\hat{\varepsilon} + \hat{p}^2/\alpha) + \hat{m}^2_{\downarrow,\Lambda}, \tag{A3}$$

$$\hat{\mathscr{P}}^{\mathrm{R}}_{\phi,\Lambda}(\hat{\omega},\hat{p}) = A_{\phi,\Lambda}[-\hat{\omega} - i\hat{\varepsilon} + \hat{p}^2/(1+\alpha)] + \hat{m}^2_{\phi,\Lambda}. \tag{A4}$$

APPENDIX B: VACUUM LIMIT

In this Appendix we derive initial conditions at $k = \Lambda$ for flow equations in the derivative expansion. The guiding principle here is to adjust the initial parameters so as to reproduce the vacuum two-body scattering correctly [45,47,61]. The initial conditions for $\alpha = 1$ have already been discussed in the Appendix in [32] and we aim here to extend their results to general α.

Let us consider a two-body system of $\uparrow$ and $\downarrow$ atoms in vacuum. In the present formalism of the FRG, this "vacuum limit" is not realized by the naive choice $\mu_\uparrow = \mu_\downarrow = 0$, because atoms are gapless only for $a < 0$ (BCS side). On the BEC side where $a > 0$, molecules are gapless, while atoms are gapped due to the bound-state formation. This means that the vacuum limit for $a > 0$ must be reached via a flow equation with $\mu = \mu_{\mathrm{v}}(a) < 0$ for atoms [45,47,61–64], where $\mu_{\mathrm{v}}(a)$ should be tuned with a (Fig. 9).

Let us therefore start with $\mu_\uparrow = \mu_\downarrow = \mu_{\mathrm{v}}(a)$. Since there is no flow of $A_\downarrow$ and $m^2_\downarrow$ in this case, one can let $A_\downarrow = 1$ and $m^2_\downarrow = -\mu_{\mathrm{v}}(a)$ for all k. The effective action in the derivative expansion at the microscopic scale $k = \Lambda$ is then given by

$$\begin{aligned}\Gamma_{k=\Lambda} = \int_P \Bigg\{ &\sum_{\sigma=\uparrow,\downarrow} \psi^*_\sigma \left[-ip_0 + \frac{\mathbf{p}^2}{2M_\sigma} - \mu_{\mathrm{v}}(a) \right] \psi_\sigma \\ &+ \phi^* \Bigg(A_{\phi,\Lambda} \left[-ip_0 + \frac{\mathbf{p}^2}{2M_\phi} - 2\mu_{\mathrm{v}}(a) \right] \\ &+ \overline{m}^2_{\phi,\Lambda}(a) \Bigg) \phi \Bigg\} + h \int_{\mathbf{x},\tau} (\psi^*_\uparrow \psi^*_\downarrow \phi + \mathrm{H.c.}),\end{aligned} \tag{B1}$$

where we have introduced the "mass term" $\overline{m}^2_{\phi,\Lambda}$ for ϕ. It follows that

$$m^2_{\phi,\Lambda} = \overline{m}^2_\phi(a) - 2A_{\phi,\Lambda}\mu_{\mathrm{v}}(a). \tag{B2}$$

We need to tune both $\overline{m}_\phi(a)$ and $\mu_{\mathrm{v}}(a)$ to recover correct IR properties in vacuum. To proceed, let us recall the fact that it is possible to compute the vacuum molecule propagator *exactly* starting from the microscopic action, (B1), using the method in [41] and [65], with the result (continued to Minkowski space-time)

$$\begin{aligned}\mathscr{P}_\phi(\omega,\mathbf{p};\mu_{\mathrm{v}}) = A_{\phi,\Lambda}\left(-\omega + \frac{\mathbf{p}^2}{2M_\phi} - 2\mu_{\mathrm{v}} \right) + \overline{m}^2_\phi(a) \\ - \frac{M_r}{\pi^2}h^2\Lambda + \frac{M_r^{3/2}}{\pi}h^2\sqrt{-\frac{\omega}{2} + \frac{\mathbf{p}^2}{4M_\phi} - \mu_{\mathrm{v}}},\end{aligned} \tag{B3}$$

where $M_r \equiv (M_\uparrow + M_\downarrow)^{-1} = \frac{\alpha}{2(1+\alpha)}$ is the reduced mass, and a sharp cutoff Λ on the spatial momentum was used to regularize a UV divergence. The parameters in (B3) can be related to the s-wave scattering length a and the effective range r_e along the lines of [45] and [47] as follows. Given the T matrix $T(q)$ for on-shell two-body scattering $(\mathbf{q}, -\mathbf{q}) \to (\mathbf{q}', -\mathbf{q}')$ in the center-of-mass frame with $|\mathbf{q}| = |\mathbf{q}'| = q$, there is a relation

$$T(q) = -\frac{h^2}{\mathscr{P}_\phi\left(-2\mu_{\mathrm{v}} + \frac{q^2}{2M_r}, \mathbf{0}; \mu_{\mathrm{v}}\right)}. \tag{B4}$$

On the other hand, the general scattering theory defines a and r_e through

$$T(q) = -\frac{2\pi}{M_r} f(\mathbf{q}) = -\frac{2\pi}{M_r} \frac{1}{-\frac{1}{a} + \frac{1}{2}r_e q^2 - iq}. \tag{B5}$$

Therefore

$$\begin{aligned}&\frac{M_r}{2\pi}h^2\left(-\frac{1}{a} + \frac{1}{2}r_e q^2 - iq \right) \\ &\overset{!}{=} \mathscr{P}_\phi\left(-2\mu_{\mathrm{v}} + \frac{q^2}{2M_r}, \mathbf{0}; \mu_{\mathrm{v}} \right) \qquad \text{(B6)} \\ &= -\frac{A_{\phi,\Lambda}}{2M_r}q^2 + \overline{m}^2_\phi(a) - \frac{M_r}{\pi^2}h^2\Lambda - i\frac{M_r}{2\pi}h^2 q. \qquad \text{(B7)}\end{aligned}$$

Comparing each term, we find

$$\overline{m}^2_\phi(a) = \frac{M_r}{\pi^2}h^2\Lambda - \frac{M_r}{2\pi a}h^2, \tag{B8}$$

$$r_e = -\frac{2\pi}{M_r^2}\frac{A_{\phi,\Lambda}}{h^2}. \tag{B9}$$

It should be stressed that these relations are correct for both signs of a. Clearly, the limit $h \to \infty$ corresponds to a broad FR ($r_e \to 0$). We remark that (B8) can also be derived by integrating (12d) directly. If we set $A_{\phi,\Lambda} = 1$ and recall (B2), it follows that we should take $m^2_{\phi,\Lambda} = \overline{m}^2_\phi(a) - 2\mu_{\mathrm{v}}(a)$ as the molecule initial condition *in the vacuum*.

In order to consider a finite-density system in general, we need to tune $\mu_\uparrow$ and $\mu_\downarrow$ away from $\mu_{\mathrm{v}}(a)$ so that the flow equation solved for $k \to 0$ yields the desired number density $n_{\uparrow,\downarrow}$. While this is a nontrivial procedure in an interacting system, things become much simpler in the case of the polaron problem: since the $\downarrow$ atoms have a vanishing density, the $\uparrow$ atoms form a *noninteracting* Fermi sea with the Fermi momentum k_F. This means that one may simply set $\mu_\uparrow = k_F^2$ without solving the complicated flow equation. In summary,

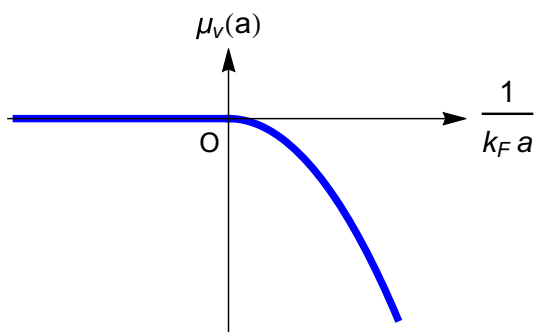

FIG. 9. The a dependence of $\mu_{\mathrm{v}}(a)$.

the molecule initial condition is given by

$$m^2_{\phi,\Lambda} = \overline{m}^2_\phi(a) - k_F^2 - \mu_\downarrow \tag{B10}$$

$$= \frac{M_r}{\pi^2}h^2\Lambda - \frac{M_r}{2\pi a}h^2 - k_F^2 - \mu_\downarrow. \tag{B11}$$

This agrees with (15) when converted to dimensionless units.

Although the functional form of $\mu_{\rm v}(a)$ is not needed in the text, we wish to include the derivation here for completeness. On the BCS side ($a < 0$), atoms are gapless physical degrees of freedom, so we simply set $\mu_{\rm v}(a) = 0$. On the BEC side ($a > 0$), we demand instead that molecules be gapless. This leads to

$$0 \stackrel{!}{=} \mathscr{P}_\phi(0,\mathbf{0};\mu_{\rm v})$$

$$= -2A_{\phi,\Lambda}\mu_{\rm v} + \overline{m}^2_\phi(a) - \frac{M_r}{\pi^2}h^2\Lambda + \frac{M_r^{3/2}}{\pi}h^2\sqrt{-\mu_{\rm v}}$$

$$= -2A_{\phi,\Lambda}\mu_{\rm v} - \frac{M_r}{2\pi a}h^2 + \frac{M_r^{3/2}}{\pi}h^2\sqrt{-\mu_{\rm v}}. \tag{B12}$$

This can be easily solved as

$$\mu_{\rm v}(a) = -\kappa^2, \tag{B13a}$$

$$\kappa = \frac{M_r^{3/2}h^2}{4\pi A_{\phi,\Lambda}}\left(-1 + \sqrt{1 + \frac{4\pi A_{\phi,\Lambda}}{M_r^2h^2a}}\right). \tag{B13b}$$

The a dependence of $\mu_{\rm v}(a)$ is illustrated in Fig. 9. We mention that $\mu_{\rm v}(a)$ is equal to half the binding energy of the stable dimer that exists at $a > 0$. Actually, in terms of r_e in (B9), we can write

$$\kappa = -\frac{1}{2\sqrt{M_r}\,r_e}\left(-1 + \sqrt{1 - \frac{2r_e}{a}}\right), \tag{B14}$$

which precisely agrees with the well-known formula in the effective range model for a narrow FR [41,42,65]. When $a \gg |r_e|$, we find $\kappa \simeq 1/(2\sqrt{M_r}a)$, thus reproducing the universal result

$$\mu_{\rm v}(a) = -\theta(a)\frac{1}{4M_ra^2} \tag{B15}$$

$$= -\theta(a)\frac{1+\alpha}{2\alpha}\frac{1}{a^2} \tag{B16}$$

for a broad FR.

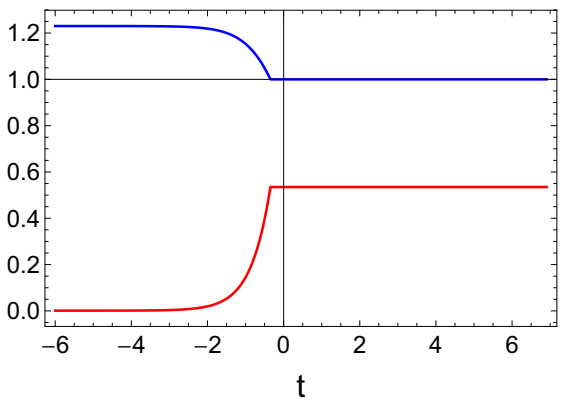

FIG. 10. Flows of $A_\downarrow$ (blue curve) and $\hat{m}^2_\downarrow$ (red curve) at unitarity for $\alpha = 1$.

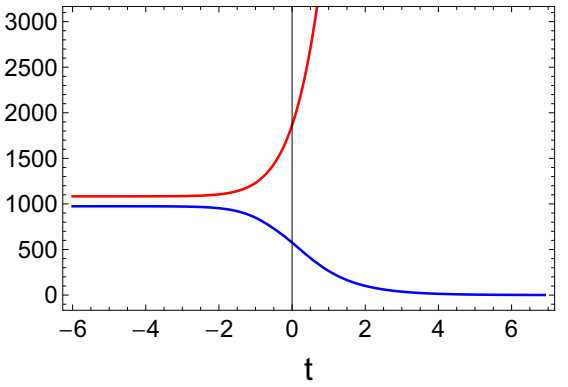

FIG. 11. Flows of A_ϕ (upper, blue curve) and $\hat{m}^2_\phi$ (lower, red curve) at unitarity for $\alpha = 1$.

APPENDIX C: FLOWING PARAMETERS

Let us examine the scale dependence of numerical solutions to (12). Figures 10 and 11 show the flows in the unitarity limit $[1/(k_Fa) = 0]$ with $\hat{h} = 300$ and $\alpha = 1$. As shown in the figures, the flow of each parameter stops at around $t = -4$, which can therefore be regarded as the $k \to 0$ limit. We also confirmed that the spectral densities have no dependence on $t_{\rm min}$ as long as $t_{\rm min} < -4$.

We observe that $\hat{m}^2_\downarrow$ flows to 0 in the IR limit, which indicates that the polaron state is the ground state at unitarity. $A_\downarrow$ is only slightly renormalized by many-body effects. By contrast, the renormalization of the molecule is significant; A_ϕ and $\hat{m}^2_\phi$ become $O(10^3)$ in the IR limit.

APPENDIX D: THE ε DEPENDENCE OF SPECTRAL FUNCTIONS

In our formulation, analytic continuation of flow equations is performed as $p_0 \Rightarrow -i(\omega + i\varepsilon)$, where ε is an infinitesimal positive constant. In numerical implementation, however, ε cannot be made arbitrarily small and it is important to understand the ε dependence of spectral functions. As a case study, we consider $1/(k_Fa) = 0.7$ with $\hat{h} = 300$ and $\alpha = 1$, where the polaron is the ground state.

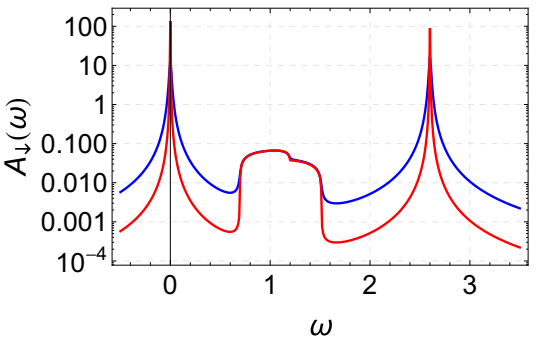

FIG. 12. Spectral function $\mathcal{A}_\downarrow(\hat{\omega},\mathbf{0})$ of an impurity at $1/(k_Fa) = 0.7$. Blue (upper) and red (lower) curves correspond to $\hat{\varepsilon} = 0.01$ and $\hat{\varepsilon} = 0.001$, respectively.

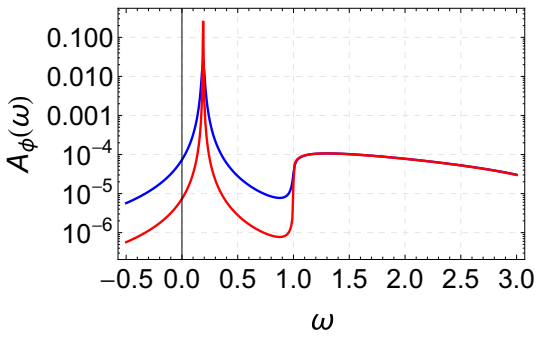

FIG. 13. Spectral function $\mathcal{A}_\phi(\hat{\omega},\mathbf{0})$ of a molecule at $1/(k_F a) = 0.7$. Blue (upper) and red (lower) curves correspond to $\hat{\varepsilon} = 0.01$ and $\hat{\varepsilon} = 0.001$, respectively.

Figure 12 shows the spectral function of a mobile impurity at a vanishing momentum. The two sharp peaks at low and high frequencies correspond to attractive and repulsive polarons, respectively. The widths of the peaks become narrower for decreasing ε, indicating that their lifetimes are infinite in our scheme. On the other hand, in between the attractive and repulsive polarons, there exists the molecule-hole continuum. This continuum spectrum is stable against variation of $\hat{\varepsilon}$.

Figure 13 shows the spectral function of a molecule at a vanishing momentum. There is a single sharp peak at low frequency, which is the molecule state and is expected to have an infinite lifetime. Similarly to the molecule-hole continuum of the polaron, the incoherent background in the high-frequency region is robust against variation of $\hat{\varepsilon}$.

APPENDIX E: TAN'S CONTACT IN A MASS-IMBALANCED FERMI GAS

Here, we discuss the so-called Tan's contact [66–68] in a system of mass-imbalanced fermions using the two-channel model. Our consideration is based on those in [69] and [70]. Let us consider the two-channel Hamiltonian

$$H = \int_{\mathbf{x}} \Bigg[-\sum_\sigma \psi_\sigma^* \frac{\nabla^2}{2M_\sigma}\psi_\sigma + \phi^* \left(-\frac{\nabla^2}{2M_\phi} + \overline{m}_\phi^2(a) \right)\phi + h(\psi_\uparrow^*\psi_\downarrow^*\phi + \text{H.c.}) \Bigg], \tag{E1}$$

where $\overline{m}_\phi^2(a)$ is the mass term introduced in (B8). Then Tan's energy relation [66] can be immediately obtained by considering the expectation value of the above Hamiltonian, which indeed corresponds to the one discussed in [69] and [70] in the limit $M_\uparrow = M_\downarrow$.

Next, we derive the so-called adiabatic relation [67], which is important for our problem and enables us to calculate Tan's contact directly. To this end, let us recall the Feynman-Hellman theorem,

$$\frac{dE}{d\lambda} = \left\langle \frac{dH}{d\lambda} \right\rangle, \tag{E2}$$

where λ is a parameter of the Hamiltonian. By setting $\lambda = a$ and using (E1) we obtain the adiabatic relation

$$\frac{dE}{da} = \frac{C}{8\pi M_r a^2}, \tag{E3}$$

where

$$C = 4M_r^2 h^2 \int_{\mathbf{x}} \langle \phi^* \phi \rangle \tag{E4}$$

is nothing but Tan's contact. Note that the above expressions reduce to those in [69] and [70] if we set $M_\uparrow = M_\downarrow$.

[1] T. K. Mitra, A. Chatterjee, and S. Mukhopadhyay, Phys. Rep. **153**, 91 (1987).
[2] R. Feynman, *Statistical Mechanics* (Westview Press, Boulder, CO, 1998).
[3] J. Devreese and S. Alexandrov, Rep. Prog. Phys. **72**, 066501 (2009).
[4] F. Grusdt and E. Demler, arXiv:1510.04934 [cond-mat.quant-gas].
[5] G. D. Mahan, *Many-Particle Physics* (Springer, Berlin, 2000).
[6] P. Massignan, M. Zaccanti, and G. M. Bruun, Rep. Prog. Phys. **77**, 034401 (2014).
[7] Z. Lan and C. Lobo, J. Indian I. Sci. **94**, 179 (2014).
[8] A. Schirotzek, C.-H. Wu, A. Sommer, and M. W. Zwierlein, Phys. Rev. Lett. **102**, 230402 (2009).
[9] S. Nascimbène, N. Navon, K. J. Jiang, L. Tarruell, M. Teichmann, J. McKeever, F. Chevy, and C. Salomon, Phys. Rev. Lett. **103**, 170402 (2009).
[10] C. Kohstall, M. Zaccanti, M. Jag, A. Trenkwalder, P. Massignan, G. M. Bruun, F. Schreck, and R. Grimm, Nature **485**, 615 (2012).
[11] M. Koschorreck, D. Pertot, E. Vogt, B. Fröhlich, M. Feld, and M. Köhl, Nature **485**, 619 (2012).
[12] N. Prokof'ev and B. Svistunov, Phys. Rev. B **77**, 020408 (2008).
[13] N. V. Prokof'ev and B. V. Svistunov, Phys. Rev. B **77**, 125101 (2008).
[14] J. Vlietinck, J. Ryckebusch, and K. V. Houcke, Phys. Rev. B **87**, 115133 (2013).
[15] P. Kroiss and L. Pollet, Phys. Rev. B **91**, 144507 (2015).
[16] R. Combescot, A. Recati, C. Lobo, and F. Chevy, Phys. Rev. Lett. **98**, 180402 (2007).
[17] R. Combescot and S. Giraud, Phys. Rev. Lett. **101**, 050404 (2008).
[18] P. Massignan, G. M. Bruun, and H. T. C. Stoof, Phys. Rev. A **78**, 031602 (2008).
[19] R. Combescot, S. Giraud, and X. Leyronas, Europhys. Lett. **88**, 60007 (2009).
[20] C. Mora and F. Chevy, Phys. Rev. A **80**, 033607 (2009).
[21] M. Punk, P. T. Dumitrescu, and W. Zwerger, Phys. Rev. A **80**, 053605 (2009).
[22] X. Cui and H. Zhai, Phys. Rev. A **81**, 041602(R) (2010).

[23] G. M. Bruun and P. Massignan, Phys. Rev. Lett. **105**, 020403 (2010).
[24] P. Massignan and G. M. Bruun, Eur. Phys. J. D **65**, 83 (2011).
[25] C. J. M. Mathy, M. M. Parish, and D. A. Huse, Phys. Rev. Lett. **106**, 166404 (2011).
[26] C. Trefzger and Y. Castin, Phys. Rev. A **85**, 053612 (2012).
[27] C. Wetterich, Phys. Lett. B **301**, 90 (1993).
[28] T. R. Morris, Int. J. Mod. Phys. A **9**, 2411 (1994).
[29] J. Berges, N. Tetradis, and C. Wetterich, Phys. Rep. **363**, 223 (2002).
[30] B. Delamotte, Lect. Notes Phys. **852**, 49 (2012).
[31] W. Metzner, M. Salmhofer, C. Honerkamp, V. Meden, and K. Schonhammer, Rev. Mod. Phys. **84**, 299 (2012).
[32] R. Schmidt and T. Enss, Phys. Rev. A **83**, 063620 (2011).
[33] J. P. Blaizot, R. Mendez Galain, and N. Wschebor, Phys. Lett. B **632**, 571 (2006).
[34] H. Vidberg and J. Serene, J. Low Temp. Phys. **29**, 179 (1977).
[35] K. Kamikado, N. Strodthoff, L. von Smekal, and J. Wambach, Phys. Lett. B **718**, 1044 (2013).
[36] K. Kamikado, N. Strodthoff, L. von Smekal, and J. Wambach, Eur. Phys. J. C **74**, 2806 (2014).
[37] R.-A. Tripolt, N. Strodthoff, L. von Smekal, and J. Wambach, Phys. Rev. D **89**, 034010 (2014).
[38] R.-A. Tripolt, L. von Smekal, and J. Wambach, Phys. Rev. D **90**, 074031 (2014).
[39] R. Bulla, T. A. Costi, and T. Pruschke, Rev. Mod. Phys. **80**, 395 (2008).
[40] J. Berges and D. Mesterhazy, Nucl. Phys. B, Proc. Suppl. **228**, 37 (2012).
[41] V. Gurarie and L. Radzihovsky, Ann. Phys. **322**, 2 (2007).
[42] E. Braaten, M. Kusunoki, and D. Zhang, Ann. Phys. **323**, 1770 (2008).
[43] J. F. Nicoll and T. S. Chang, Phys. Lett. A **62**, 287 (1977).
[44] J. M. Pawlowski and N. Strodthoff, Phys. Rev. D **92**, 094009 (2015).
[45] S. Diehl, S. Floerchinger, H. Gies, J. M. Pawlowkski, and C. Wetterich, Ann. Phys. **522**, 615 (2010).
[46] J. Braun, J. Phys. G **39**, 033001 (2012).
[47] I. Boettcher, J. M. Pawlowski, and S. Diehl, Nucl. Phys. Proc. Suppl. **228**, 63 (2012).
[48] M. Jarrell and J. E. Gubernatis, Phys. Rep. **269**, 133 (1996).
[49] P. Massignan, Europhys. Lett. **98**, 10012 (2012).
[50] J. M. Pawlowski, M. M. Scherer, R. Schmidt, and S. J. Wetzel, arXiv:1512.03598 [hep-th].
[51] J. E. Baarsma, J. Armaitis, R. A. Duine, and H. T. C. Stoof, Phys. Rev. A **85**, 033631 (2012).
[52] O. Goulko, A. S. Mishchenko, N. Prokof'ev, and B. Svistunov, Phys. Rev. A **94**, 051605(R) (2016).
[53] R. Bishop, Ann. Phys. **78**, 391 (1973).
[54] C. Lobo, A. Recati, S. Giorgini, and S. Stringari, Phys. Rev. Lett. **97**, 200403 (2006).
[55] S. Pilati and S. Giorgini, Phys. Rev. Lett. **100**, 030401 (2008).
[56] M.-G. Hu, M. J. Van de Graaff, D. Kedar, J. P. Corson, E. A. Cornell, and D. S. Jin, Phys. Rev. Lett. **117**, 055301 (2016).
[57] N. B. Jørgensen, L. Wacker, K. T. Skalmstang, M. M. Parish, J. Levinsen, R. S. Christensen, G. M. Bruun, and J. J. Arlt, Phys. Rev. Lett. **117**, 055302 (2016).
[58] W. Zwerger, *The BCS-BEC Crossover and the Unitary Fermi Gas* (Springer Science & Business Media, New York, 2011), Vol. 836.
[59] G. Modugno, G. Roati, F. Riboli, F. Ferlaino, R. J. Brecha, and M. Inguscio, Science **297**, 2240 (2002).
[60] C. Ospelkaus, S. Ospelkaus, K. Sengstock, and K. Bongs, Phys. Rev. Lett. **96**, 020401 (2006).
[61] S. Diehl, H. Gies, J. M. Pawlowski, and C. Wetterich, Phys. Rev. A **76**, 053627 (2007).
[62] S. Diehl and C. Wetterich, Nucl. Phys. B **770**, 206 (2007).
[63] S. Diehl, H. Gies, J. M. Pawlowski, and C. Wetterich, Phys. Rev. A **76**, 021602 (2007).
[64] S. Diehl, H. C. Krahl, and M. Scherer, Phys. Rev. C **78**, 034001 (2008).
[65] J. Levinsen and D. S. Petrov, Eur. Phys. J. D **65**, 67 (2011).
[66] S. Tan, Ann. Phys. **323**, 2952 (2008).
[67] S. Tan, Ann. Phys. **323**, 2971 (2008).
[68] S. Tan, Ann. Phys. **323**, 2987 (2008).
[69] E. Braaten and L. Platter, Phys. Rev. Lett. **100**, 205301 (2008).
[70] E. Braaten, D. Kang, and L. Platter, Phys. Rev. A **78**, 053606 (2008).